Journal of Environmental Radioactivity 268-269 (2023) 107247

Contents lists available at ScienceDirect

Journal of Environmental Radioactivity

journal homepage: www.elsevier.com/locate/jenvrad

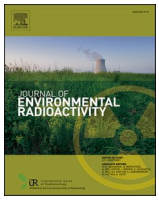

^{210}Pb-based dating of recent sediments with the χ-mapping version of the Constant Sediment Accumulation Rate (CSAR) model

J.M. Abril-Hernández *

Departamento de Física Aplicada I, Universidad de Sevilla, Spain

ARTICLE INFO

Keywords:
^{210}Pb dating
Recent sediments
χ-mapping models
Constant sedimentation
CSAR model

ABSTRACT

The ^{210}Pb-based method aims at determining the absolute age of recent sediments on the centennial scale. A family of models assumes that at the sediment-water interface the flux of unsupported ^{210}Pb (^{210}Pb$_{exc}$), F, relates to its initial activity concentration, A_o, and the mass sedimentation rate, w, as: $F = A_o w$. Additional specific assumptions that allow for analytical formulations of the models are: i) constant A_o (CIC), constant F (CF), and constant F with constant w (CFCS). A model with constant w (CSAR) was suggested for completeness but never used because of the lack of a suitable analytical formulation. The TERESA model assumes random and independent variability for A_o and w, described by normal distributions. It systematically generates a large number (~10^5) of potential solutions, whose performance for fitting the empirical ^{210}Pb$_{exc}$ profile is quantified through the χ-function. This work aims to adapt the above methodology to formulate the χ-mapping version of the CSAR model. The performance of the model is evaluated with a set of synthetic and real cores for which an independent chronology is available. CSAR is able to capture the mean sedimentation rate from the ^{210}Pb$_{exc}$ data and provides reliable chronologies and paleorecords of A_o, useful for tracking past changes in sedimentary conditions. CSAR provides an interesting different perspective for researchers working with ^{210}Pb-based dating of recent sediments.

1. Introduction

The ^{210}Pb-based method has been widely used during the last five decades for determination of absolute ages in recent sediments at centennial scale (e.g., Koide et al., 1973; Caroll and Lerche, 2003; Appleby, 2008; Mabit et al., 2014; Arias-Ortiz et al., 2018). The technique relays on the geochemical cycling of ^{210}Pb ($T_{1/2}$ = 22.3 a) in nature (Robbins, 1978), and it uses the ^{210}Pb found in excess (labelled hereafter as ^{210}Pb$_{exc}$) with respect to its parent radionuclide ^{226}Ra along the sediment core.

In the porous medium of aquatic sediments, ^{210}Pb tends to be strongly bound to solids (IAEA, 2004), which justifies the common approach of considering the sediment as a continuous medium characterised by its bulk density to study the space-temporal changes of the concentrations of ^{210}Pb$_{exc}$. For the same reason, ^{210}Pb$_{exc}$ reaches the sediment-water interface (SWI) mostly associated with mass flows, with an initial mass activity concentration A_o. The deposition of particle-bound ^{210}Pb$_{exc}$ on the previously existing material is generally a reliable condition. Post-depositional reworking of solids requires forcing agents such as bioturbation or tidal cycles of resuspension and deposition, which are absent in many study cases. Under these conditions, the mass sediment accumulation rate (referred as SAR, and denoted with the symbol w) and A_o relates with the ^{210}Pb$_{exc}$ flux at the SWI, F, by the mathematical condition of continuity:

$$F = A_o w \tag{1}$$

In the above sedimentary scenario, after deposition ^{210}Pb$_{exc}$ mass activity concentrations only decrease by radioactive decay while the sediment accretes with the accumulation of new materials. This requires the continuity of the sedimentary sequence (i.e., the absence of erosion).

The above assumptions can be violated in some sedimentary scenarios. Examples are: i) the existence of post-depositional redistribution (e.g., Robbins and Edgington, 1975; Abril et al., 1992; Laissaoui et al., 2008); ii) non-ideal deposition of fluxes, when a mobile fraction of the ^{210}Pb$_{exc}$ flux undergoes a fast distribution in depth (Abril and Gharbi, 2012); iii) polyphasic porous media (e.g., when rhizospheres shows different uptake and mobility than mineral solids; Iurian et al., 2021). In the most general case, the long-term fate of tracer elements in the porous

* Corresponding author. ETSIA, Universidad de Sevilla, Carretera de Utrera km1 D.P, 41013, Sevilla, Spain.
E-mail address: jmabril@us.es.

https://doi.org/10.1016/j.jenvrad.2023.107247
Received 26 May 2023; Received in revised form 14 July 2023; Accepted 20 July 2023
Available online 25 July 2023

medium of sediments is governed by the kinetics of their uptake by solids and by physical transport through the pore fluid (Abril and Barros, 2022; Abril, 2023).

A fundamental feature of the ^{210}Pb-based dating method is that the empirical data (consisting of the $^{210}Pb_{exc}$ mass activity concentrations along the core depth) do not unambiguously define a chronology (an age-depth relationships). Even for the simplest but quite common sedimentary conditions behind Eq. (1), it can be demonstrated that there are an infinite number of chronologies that are mathematically exact solutions for any given dataset, independently of the accuracy of the analytical measurements (Abril, 2015).

Selecting a single chronology (more properly constraining it with the analytical errors) from the above infinite set of possibilities is only possible after introducing additional assumptions on F, w and/or A_o. The most widely used model assumes constant flux, leading to the CF model, with two known versions: its Bayesian formulation, the PLUM model (Aquino-López et al., 2018), and the classical CRS model, which includes the additional assumption of a steady-state total inventory of $^{210}Pb_{exc}$ (Appleby and Oldfield, 1978). A less popular assumption is that of a constant A_0 (the CIC model) (Goldberg, 1963). The CFCS model assumes that F and w are constant over time (Robbins, 1978). These assumptions are mathematically convenient choices, since they allow for analytical solutions. However, this does not ensure their physical reliability. A detailed presentation of these models can be seen in Sánchez-Cabeza and Ruíz-Fernández (2012), and a R software package can be seen in Bruel and Sabatier (2020).

A model with constant sedimentation was first considered by Robbins (1978) for the sake of completeness of the cases inferred from Eq. (1). A brief presentation can be found in Sánchez-Cabeza and Ruíz--Fernández (2012). The mass activity concentration of $^{210}Pb_{exc}$ found in the sediment slice of index k, that is at a mass depth m, relates with the flux F_k that it received when was forming at the SWI:

$$A_k = \frac{F_k}{w} e^{-\lambda \frac{m}{w}}, \tag{2}$$

where λ is the radioactive decay constant for ^{210}Pb. These authors noticed that this model can only be used if the values of the fluxes to the sediment surface are known during the interest period.

A trivial application of the model is possible when w is known from a time mark such as the ^{137}Cs peaks related to the history of its atmospheric deposition (e.g., Iurian et al., 2021). However, this model has never been used to establish a chronology using only the ^{210}Pb data.

The basic formulation of the TERESA model (Abril, 2016) uses normal and independent distributions for A_0 and w, a sorting algorithm for the arrangement of their values along the core, and the mapping of the χ-function to find the parameter values for the normal distributions that best fit the empirical profile (the absolute minimum of χ). For complex profiles, a multimodal version of TERESA was presented (Abril, 2020). Other applications of the TERESA model can be seen, among others, in Botwe et al. (2017); Klubi et al. (2017); Iurian et al. (2021); and Abril (2022).

This work aims at adapting the above methodology of TERESA to formulate the χ-mapping version of the CSAR model. The performance of the model will be evaluated with a set of synthetic and real cores, for which an independent chronology is available.

2. Methods

2.1. The χ-mapping CSAR model

The mass depth scale, m, the dry mass per unit area accumulated from the SWI, remains invariant under natural compaction and sediment shortening (during the coring, storage, and extrusion processes). It is a physically meaningful and appropriate scale for formulating the advection-diffusion equation and ^{210}Pb-based dating models (Abril, 2003).

For a core sectioned into n slices, the empirical dataset is a set of pairs $(A_k, \Delta m_k)$, with k being an integer number ranging from 1 to n. A_k is the mass activity concentration of $^{210}Pb_{exc}$ in the slice of index k, and $\Delta m_k = \rho_{b,k} \Delta z_k$, with $\rho_{b,k}$ the bulk density of the slice, and Δz_k its depth thickness. Both magnitudes are known with their respective analytical uncertainties, $\sigma_{A,k}$ and $\sigma_{m,k}$.

The slice of index k was formed at the SWI during a time interval ΔT_k, with a time-averaged SAR, w_k, a mean initial activity concentration $A_{0,k}$, and a mean flux $F_k = A_{o,k} w_k$. If the n pairs of values $(A_{o,k}, w_k)$ were known and sorted in the true sequence of the formation of the subsequent slices, then the chronology and the decay-corrected profile that matches the empirical one can be estimated as follows:

$$\Delta T_k = \frac{\Delta m_k}{w_k} \; ; \; T_k = T_{k-1} + \Delta T_k \tag{3a}$$

$$A_k = A_{o,k} \frac{1 - e^{-\lambda \Delta T_k}}{\lambda \Delta T_k} \, e^{-\lambda T_{k-1}} \tag{3b}$$

The pairs $(A_{o,k}, w_k)$ are unknown, but the n $A_{0,k}$ values follow a certain statistical distribution. The method can be applied to other choices of probability distribution functions, but here it will be assumed that $A_{0,k}$ values are normally distributed with (unknown) mean, $\overline{A}_o$, and relative standard deviation s_A ($s_A = \sigma_A / \overline{A}_o$). CSAR also assumes that w_k takes a constant (but unknown) value $\overline{w}$.

The first step is to adopt the initial tentative values for the above three parameters. Then, it is possible generating a sample of size n of $A_{o,i}$ values following such a normal distribution. A practical procedure, but not the only possible, is to use the so-called *canonical representative sample* of size n from a normal typified distribution $\mathcal{N}(0,1)$. It comprises the n z_i values generated from equal intervals in the cumulative distribution function (CFD) centred in $\frac{1}{2}$, and then randomly sorted, as described in detail in Abril (2016, 2020). This ensures a mean value of zero and a standard deviation of 1, even for samples of small size. Then, the sample of n $A_{o,i}$ values is

$$A_{o,i} = \overline{A}_o (1 + s_A z_i) \; ; \; i = 1, 2, \ldots n \tag{4}$$

The set of n pairs $(A_{o,i}, \overline{w})$ is referred as to *a solver*. By systematically varying the initial estimate of the $\overline{A}_o$, $\overline{w}$, and s_A values one can generate a very large number ($\sim 10^5$-10^6) of potential solvers for selecting the one with the best performance.

For each solver, the n pairs $(A_{o,i}, \overline{w})$ must be conveniently sorted along the core to get the best possible agreement with the empirical profile. To this end, the sorting algorithm proposed by Abril (2016) is used in this work (the code can be seen as supplementary material in Abril, 2020). It uses a top to down approach. For the first slice ($k = 1$), it applies Eq. (3) with the n pairs to find which of them best fit the empirical value A_1. The pair is stored as part of the solution, and the process continues with the second slice and the remaining $n - 1$ pairs, and so on. This method has shown its practical use, although other programming approaches are possible.

After sorting, Eq. (3) provides the decay-corrected profile generated from the solver, denoted as A_k^*. The global performance of the solver can be quantified through the Q^2 function:

$$Q^2 = \sum_{k=1}^{n} \frac{\left(A_k^* - A_k\right)^2}{\sigma_{A,k}^2} \tag{5}$$

The $\chi^2 = Q^2 / f$ function involves the number of degrees of freedom, $f = n - p + 1$, with p the number of free parameters in the model. The best solution for the problem will be that solver that minimizes Q^2 (or χ). Intuitively, a value $\chi = 1$ means that the distances between the predictions and measurements are of the same size as the analytical uncertainties. The model output is a chronology, the value of SAR, and the temporal records of the initial activity concentrations and fluxes.

In some complex cases, the χ-function may comprise an absolute minimum and several secondary minima. Therefore, the algorithm or the method for walking on the χ-hypersurface must be replicated with different starting points to ensure a robust identification of the absolute minimum.

The uncertainties in the fitting parameters can be estimated from the curvature of the parametric lines at the absolute minimum, according to Bevington and Robinson (2003). Thus, for a generic parameter, x,

$$\sigma_x^2 = 2\left(\frac{\partial^2 Q^2}{\partial x^2}\right)^{-1}. \quad (6)$$

The propagated uncertainties in the chronology can be estimated by the following general rule:

$$\sigma_{T,k}^2 = \left(\frac{\partial T_k}{\partial \overline{A}_o}\right)^2 \sigma_A^2 + \left(\frac{\partial T_k}{\partial \overline{w}}\right)^2 \sigma_w^2 + \left(\frac{\partial T_k}{\partial s_A}\right)^2 \sigma_{sA}^2 \quad (7)$$

2.2. Application to synthetic and real cores

A set of cores has been selected for the application and testing of the model. In all the cases, an independent chronology is used for model validation. This provides a more robust test, since the use of a single or a few independent chronostratigraphic markers, as suggested by Smith (2001), has shown to be of ambiguous interpretation or a weak constraint in some cases (see Abril, 2004, 2019).

Core C1 is a varved sediment sampled in 2007 in Lake Lazduny (northeastern Poland), at 20 m depth (data from Tylmann et al., 2013 - their core LAZ 07/02). It was included in the survey by Abril and Brunskill (2014) –their core C9. It comprises $n = 14$ slices.

Core C2 is a varved sediment sampled in April 1999 in the Pettaquamscutt River basin (Rhode Island, Northeast USA), 41°30′N, 71°26′W, at 19.5 m depth (data from Lima et al., 2005). The reconstructed paleorecords of F, w and A_o were presented in Abril (2020). It comprises $n = 23$ slices.

Core C3 is a varved sediment sampled in April 2011 in Lake Kevojärvi, Finland (69°45′N, 27°00' E) at 35 m water depth (data from Haltia et al., 2021). The raw data used (from their Table 1 and 2) have been: mid-varve age, varve bottom depth, dry bulk density, total ^{210}Pb (with analytical uncertainties) and ^{226}Ra (with uncertainties). ^{210}Pb$_{exc}$ has been estimated by subtracting ^{226}Ra from the total ^{210}Pb layer-by-layer basis (interpolations were necessary for few missing ^{226}Ra measurements). This core comprises $n = 53$ slices.

Core C4 is a synthetic core generated following the methodology presented in Abril (2016). Briefly, $n = 34$ values of A_0 and SAR were generated as in Eq. (4) by using $\overline{A}_o = 100$ Bq kg^{-1}; $s_A = 0.30$; $\overline{w} = 0.20$ g cm^{-2}a^{-1}; $s_w = 0.30$, and then randomly sorted. They represented the sedimentary conditions for a core comprising 34 slices of 1 cm thick each. A realistic bulk density profile was used to generate the mass thickness of each slice. This, along with the value of w_i, allows for estimating the time interval in each slice, and then the chronology. This last is used to convert (through radioactive decay) $A_{o,i}$ into the 'empirical' ^{210}Pb$_{exc}$ mass activity concentrations. Uncertainties of 10% plus a constant contribution were arbitrarily ascribed.

2.3. Software

A set of codes has been written in the BASIC language using QuickBasic software and run under an MSDOS emulator. The TERESA codes are available for scientific evaluation as supplementary material in Abril (2020). The adaptations required for the χ-mapping versions of the CSAR model are relatively simple to implement from these codes and the methods presented above. The available package also includes an Excel file with the method to generate the canonical representative distributions of varying sizes from $\mathcal{N}(0,1)$.

3. Results and discussion

Figs. 1–4 and Table 1 summarise the results for the application of the CSAR model to the selected cores.

The empirical ^{210}Pb$_{exc}$ versus mass depth profiles show a varying

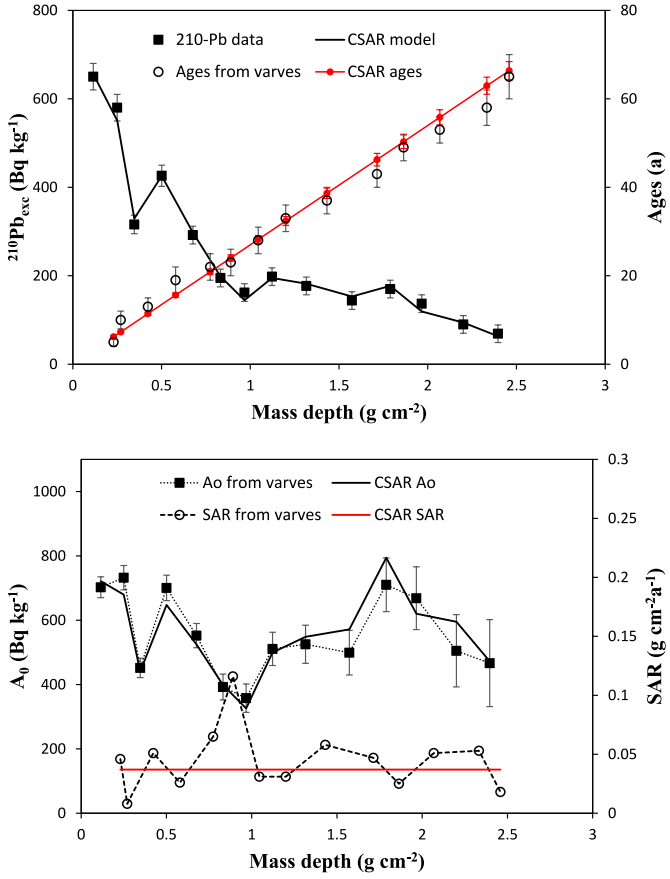

Fig. 1. Application of the CSAR model to core C1 (Lake Lazduny). Upper panel: ^{210}Pb$_{exc}$ versus mass depth, with1-σ analytical uncertainties. The continuous line is the best-fit obtained with CSAR (the line connects the model values, ascribed to the centre of each slice). The ages from the varves and from the model are depicted in the secondary Y-axis. For the latter, the error bars are 1-σ propagated uncertainties (by Eq. (7)). Lower panel: Initial activity concentrations and SARs estimated from varves and for direct output of the CSAR model.

Table 1
Fitted model parameters for the application of the CSAR model, and χ values.

Core	$\overline{A}_o$ (Bq kg^{-1})			$\overline{w}$ (g cm^{-2}a^{-1})			s_A			χ
C1	560	±	8	0.0370	±	0.0012	0.234	±	0.002	0.57
C2	514.6	±	1.6	0.0601	±	0.0002	0.190	±	0.002	0.51
C3	320.0	±	1.6	0.1250	±	0.0007	0.378	±	0.008	0.56
C4	104	±	6	0.1700	±	0.0014	0.318	±	0.015	0.19

Uncertainties in the fitted parameters have been estimated by Eq. (6).

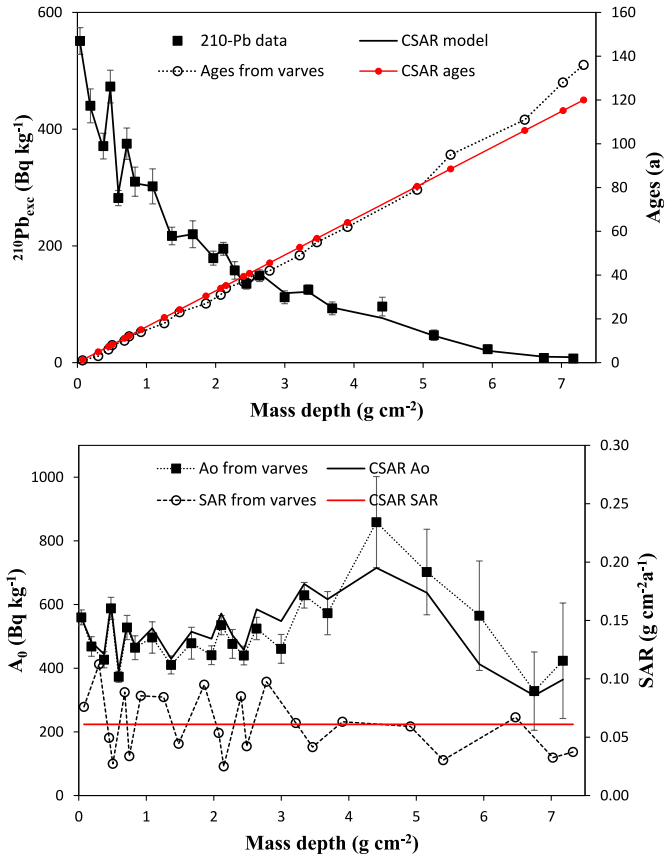

Fig. 2. As in Fig. 1, but with the application of the CSAR model to the core C2 (Pettaquamscutt River basin).

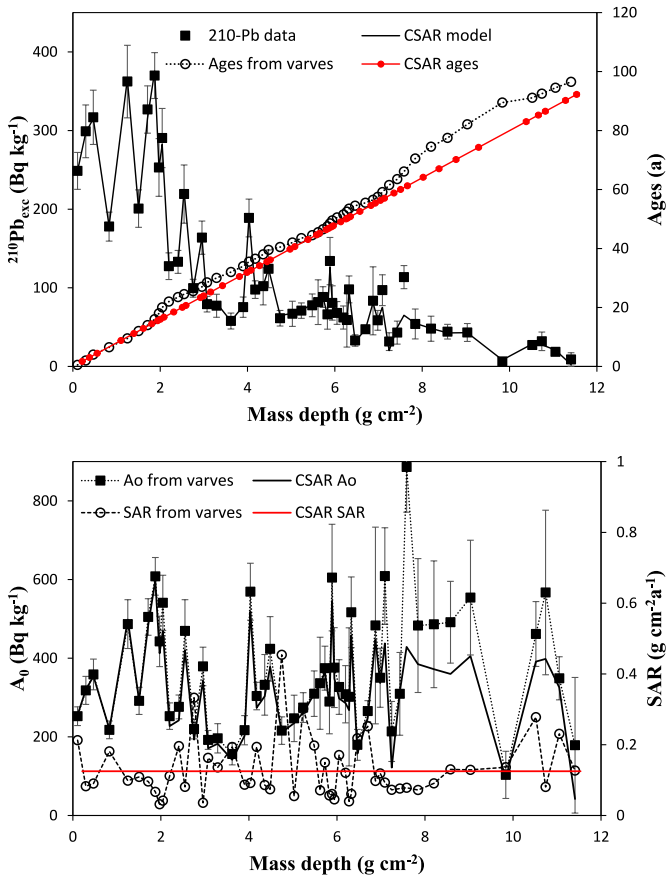

Fig. 3. As in Fig. 1, but with the application of the CSAR model to core C3 (Lake Kevojärvi).

degree of irregularities over the ideal pattern of an exponential decrease. They range from moderate (cores C1 and C2) to very large irregularities (cores C3 and C4). In all cases, the CSAR model provided solutions in excellent agreement with the empirical data, with χ values < 0.6 (see Table 1). The fitted parameters were well constrained in all cases, as shown in Table 1.

The varve chronology for core C1 was provided with associated uncertainties, which are reported in Fig. 1. As seen in that figure, the model chronology is in rather good agreement with the one from varves. The CSAR model only captures a mean value for SAR, but is able to reasonably reproduce the temporal variability of the initial activity concentrations (Fig. 1), which is roughly randomly distributed along the time line.

With core C2 (Fig. 2) the CSAR model also provides an excellent fit to the $^{210}Pb_{exc}$ data, and the model chronology is overall in good agreement with that from varves, although with a moderate departure for older ages. The model also captures the major features of the temporal variability of A_o. In this case, the variability is not purely random and has a markedly different structure in older layers. A more detailed study of this core in terms of piecewise versions of the CF and TERESA models can be seen in Abril (2020).

Fig. 3 summarises the results for core C3. Despite the complexity of the $^{210}Pb_{exc}$ profile, CSAR produces an excellent fit ($\chi = 0.56$), and a reasonable proxy of the chronology of the varves (Fig. 3). In this case, the paleorecords of initial activity concentrations from varves show strong variability with a sequence of periods with high and low values of A_o. CSAR is able to capture the major features of this variability although with poorer agreement in deeper layers. CSAR also captures the mean value of SAR.

The solution provided by CSAR for the synthetic core C4 is in particular good agreement with the $^{210}Pb_{exc}$ profile ($\chi = 0.19$), and the model chronology closely matches the synthetic one (Fig. 4). The model captures a mean SAR value of 0.17 g cm^{-2}a^{-1}. It is a time-averaged value over the whole length of the core, and it is not in contradiction with the stated arithmetic mean (0.20 g cm^{-2}a^{-1}) of the values of the 34 slices, which are of varying mass thickness and with w_i values deviating from the mean, so that they have associated varying time intervals. In fact, the average SAR for the synthetic core can easily be calculated as the mass depth of the deepest layer divided by its synthetic age (0.179 g cm^{-2}a^{-1}).

The propagated uncertainties (from Eq. (7)) were below 4% in core C1 and below 1% for the other cores. They inform the effects of the computations involved in the application of the model. However, there are always nonquantifiable model errors that are deviations of the model ages from the true chronology due to the partial or null achievement of some of the model assumptions (Abril, 2022), as observed in the studied cases, in Figs. 1–4. The CSAR model assumes a constant SAR, while the sedimentation rates inferred from the varve chronology show a large temporal variability (Figs. 1–4). Other sources of model errors are the assumption of normally distributed A_o, and the particular choice for generating solvers (Eq. (4)), which only can provide a proxy for the true (but unknown) distributions. However, CSAR has shown its ability to compensate for positive and negative deviations in chronology in the studied cases, where the temporal variability of A_0 and SAR were roughly randomly distributed along the time line (Figs. 1–4). This result is in agreement with previous findings (Abril 2019, 2020) showing that under random temporal variability in fluxes, the CF and CFCS models are able to compensate positive and negative deviations, producing chronologies that keep close to the true solution (when known from varves and in synthetic cores).

Going into detail, in the studied cores, the largest model errors in the

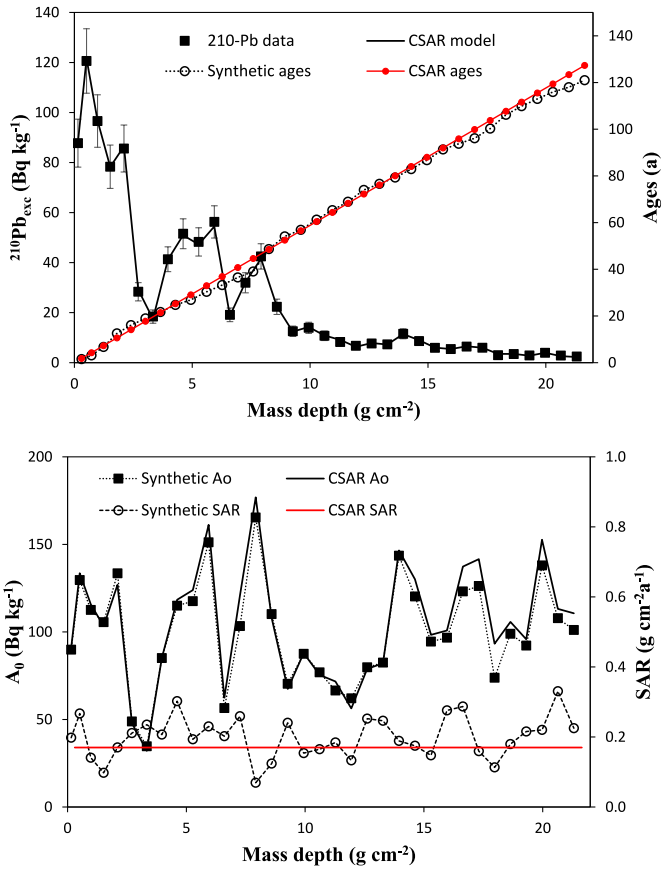

Fig. 4. As in Fig. 1, but with the application of the CSAR model to the synthetic core C4. Here, model outputs are compared against the synthetics chronology, A_o and SAR.

chronologies appeared in the deeper region of core C2, linked to a non-random variability in A_o (Fig. 2, Abril, 2020), and in core C3, where the variability in A_o showed a pseudo-periodic structure with high and low values, which was difficult for the model to balance (Fig. 3).

It is worth noting that the sorting algorithm used, which runs from top to bottom, necessarily has a poorer performance for older (deeper) layers. This effect interplays with the cumulative behaviour of model errors during transects with continuous trends of increase or decrease.

It has been shown (Abril, 2022) that model errors differently affect the output paleorecords of SARs and A_o, being the former largely affected by spurious fluctuations than make them unusable for tracking past changes in sedimentary conditions. On the contrary, A_o are less affected by model errors, so they are the suitable magnitude for the above goal. For the same reason, SARs and A_o differently contribute to the value of A_k in Eq. (3). After a second order expansion ($\lambda\Delta T_k \ll 1$),

$$A_k \cong A_{o,k} e^{-\lambda T_{k-1}} \left(1 - \frac{\lambda}{2}\frac{\Delta m_k}{w_k}\right). \quad (8)$$

Thus, once the mean values of A_o and w have been captured, a fluctuation by a factor two in $A_{o,k}$ automatically translates into a change of equal size in A_k, while such a change in w_k yields to changes of the order of 2%–5%. As a consequence, those models allowing for varying A_o (CF, CSAR, and TERESA) have the chance of producing solutions in close agreement with the empirical $^{210}Pb_{exc}$ profiles, as well as reliable paleorecords of A_o, as shown in this work.

The synthetic core C4 gives the opportunity to observe how the prescribed variability in SARs, which by the main assumption of the CSAR is ignored, is compensated by tiny deviations in the paleorecords of A_o, which are slightly higher than the synthetic records in deeper layers.

The model assumptions may not reliably describe the true behaviour of F, A_0 and w in the sedimentary system studied, but this does not necessarily invalidate them. The poor or null accomplishment of model assumptions results in model errors. Models show the capability of compensating positive and negative deviations from the true chronology when the temporal variability of the above magnitudes is randomly distributed along the time line. A_0 and w differently contribute to the model chronology, the former being the dominant one. Thus, those models allowing for variability in A_0 can show better performance. This is the case for the CSAR model, which in its χ-mapping version represents a new tool for researchers deading with the ^{210}Pb-based dating of recent sediments. It is necessary to gain more experience with its application to a large variety of scenarios to discover its potentials and limitations, and the insights it can provide when used in combination with other dating models. Especially, it should be noted that, although conceptually the CSAR model is a particular case of the TERESA model, there are some practical advantages to support its combined use: i) CSAR defines 3D χ-hypersurfaces (from Eq. (5)) which are simpler and smoother than the 4D ones from TERESA, which can be helpful for identifying the absolute minimum in complex cases; ii) the concordance of their chronologies may inform on the occurrence of sedimentary conditions with randomly distributed variability in SAR.

4. Conclusions

The χ-mapping version of the CSAR model has been presented. It arises as a particular case of the TERESA model, restricted by the condition of a constant SAR (set in the software as a null standard deviation in w).

This work has presented the first applications of this model using exclusively $^{210}Pb_{exc}$ data and the mass depth scale in the sediment core.

The model has shown good performance with real and synthetic cores for which an independent chronology (synthetic or from varves) was available. It produced solutions that fitted the experimental profiles with χ values < 0.6, and model ages, in general, in good agreement with the independent chronology.

The CSAR model is able to output paleorecords of initial activity concentrations that are in good agreement with those inferred from the varve or synthetic chronologies, so they are suitable for tracking past changes in sedimentary conditions.

The studied cores show large temporal variability in both, A_o and w, and then in fluxes. However, such a variability was more or less randomly distributed along the time line or showed periods of increase mostly compensated by others of decrease (core C3). Under these conditions, CSAR is able to compensate for model errors in the chronology, which is consistent with similar findings for the CRS and CFCS models.

CSAR complements the set of classical models. As all the models, it can be applied separately, subjected to validation with at least an independent chronostratigraphic marker. As a practical advantage, it can be applied to complex profiles without a complete recovery of the total inventory, and it is simpler to use than the TERESA model. The combination with other models can provide useful information on the prevailing sedimentary conditions. Thus, the CSAR model provides an interesting new perspective for researchers working with the ^{210}Pb-based dating of recent sediments.

Declaration of competing interest

The authors declare that they have no known competing financial interests or personal relationships that could have appeared to influence the work reported in this paper.

Data availability

Data will be made available on request.

References

Abril, J.M., 2003. A new theoretical treatment of compaction and the advective-diffusive processes in sediments. A reviewed basis for radiometric dating models. J. Paleolimnol. 30, 363–370. https://doi.org/10.1023/B:JOPL.0000007220.16908.d4.

Abril, J.M., 2004. Constraints on the use of ^{137}Cs as a time-marker to support CRS and SIT chronologies. Environ. Pollut. 129, 31–37. https://doi.org/10.1016/j.envpol.2003.10.004.

Abril, J.M., 2015. Why would we use the Sediment Isotope Tomography (SIT) model to establish a ^{210}Pb-based chronology in recent-sediment cores? J. Environ. Radioact. 143, 40–46. https://doi.org/10.1016/j.jenvrad.2015.02.008.

Abril, J.M., 2016. A ^{210}Pb-based chronological model for recent sediments with random entries of mass and activities: model development. J. Environ. Radioact. 151, 64–74. https://doi.org/10.1016/j.jenvrad.2015.09.018.

Abril, J.M., 2019. Radiometric dating of recent sediments: on the performance of ^{210}Pb-based CRS chronologies under varying rates of supply. Quat. Geochronol. 51, 1–14. https://doi.org/10.1016/j.quageo.2018.12.003.

Abril, J.M., 2020. Multimodal-TERESA, a ^{210}Pb-based radiometric dating model for recent sediments under largely varying rates of supply. Quat. Geochronol. 55, 101032 https://doi.org/10.1016/j.quageo.2019.101032.

Abril, J.M., 2022. On the use of ^{210}Pb-based records of sedimentation rates and activity concentrations for tracking past environmental changes. J. Environ. Radioact. 244–245, 106823 https://doi.org/10.1016/j.jenvrad.2022.106823.

Abril, J.M., 2023. Kinetic reactive transport explains distinct subsurface deposition patterns of pollutants in sediments. The case of the Sellafield-derived ^{236}U, ^{137}Cs and ^{239,240}Pu in the Esk Estuary, UK. Environ. Pollut. 323, 121244 https://doi.org/10.1016/j.envpol.2023.121244.

Abril, J.M., Barros, H., 2022. Modelling the kinetic reactive transport of pollutants at the sediment-water interface. Applications with atmospheric fallout radionuclides. J. Environ. Radioact. 242, 106790 https://doi.org/10.1016/j.jenvrad.2021.106790.

Abril, J.M., Brunskill, G.J., 2014. Evidence that excess ^{210}Pb flux varies with sediment accumulation rate and implications for dating recent sediments. J. Paleolimnol. 52, 121–137. https://doi.org/10.1007/s10933-014-9782-6.

Abril, J.M., García-León, M., García-Tenorio, R., Sánchez, C.I., El- Daoushy, F., 1992. Dating of marine sediments by an incomplete mixing model. J. Environ. Radioact. 15, 135–151.

Abril, J.M., Gharbi, F., 2012. Radiometric dating of recent sediments: beyond the boundary conditions. J. Paleolimnol. 48, 449–460. https://doi.org/10.1007/s10933-012-9622-5.

Appleby, P.G., Oldfield, F., 1978. The calculation of lead-210 dates assuming a constant rate of supply of unsupported ^{210}Pb to the sediment. Catena 5, 1–8.

Appleby, P.G., 2008. Three decades of dating recent sediments by fallout radionuclides: a review. Holocene 18 (1), 83–93. https://doi.org/10.1177/0959683607085598, 93.

Aquino-López, M.A., Blaauw, M., Christen, J.A., Sanderson, N.K., 2018. Bayesian analysis of ^{210}Pb dating. J. Agric. Biol. Environ. Stat. 23, 317–333.

Arias-Ortiz, A., Masqué, P., Garcia-Orellana, J., Serrano, O., Mazarrasa, I., Marbà, N., Lovelock, C.E., Lavery, P.S., Duarte, C.M., 2018. Reviews and syntheses: ^{210}Pb-derived sediment and carbon accumulation rates in vegetated coastal ecosystems: setting the record straight. Biogeosci. Discuss. https://doi.org/10.5194/bg-2018-78.

Bevington, P.A., Robinson, D.K., 2003. Data Reduction and Error Analysis for the Physical Sciences, third ed. McGraw-Hill, New York.

Botwe, B.O., Abril, J.M., Schirone, A., Barsanti, M., Delbono, I., Delfanti, R., Nyarko, E., Lens, P.N.L., 2017. Settling fluxes and sediment accumulation rates by the combined use of sediment traps and sediment cores in Tema Harbour (Ghana). Sci. Total Environ. 609, 1114–1125.

Bruel, R., Sabatier, P., 2020. *serac*: a R package for ShortlivEd RAdionuclide chronology of recent sediment cores. J. Environ. Radioact. 225, 106449 https://doi.org/10.1016/j.jenvrad.2020.106449.

Caroll, J., Lerche, I., 2003. Sedimentary Processes: Quantification Using Radionuclides. Elsevier, Oxford.

Goldberg, E.D., 1963. Geochronology with Pb-210. In: Proceedings of a Symposium of Radioactive Dating. International Atomic Energy Agency, Vienna, pp. 121–131.

Haltia, E., Leppänen, A.-P., Kallio, A., Saarinen, T., 2021. Sediment profile dating and reconstructing nuclear events from annually laminated lake sediments in northern Finland. J. Environ. Radioact. 233, 106611 https://doi.org/10.1016/j.jenvrad.2021.106611.

IAEA, 2004. Sediment distribution coefficients and concentration factors for biota in the marine environment. In: International Atomic Energy Agency Technical Report Series 422 (Vienna, Austria).

Iurian, A.R., Millward, G., Blake, W., Abril Hernández, J.M., 2021. Fine-tuning of ^{210}Pb-based methods for dating vegetated saltmarsh sediments. Quat. Geochronol. 62, 101153 https://doi.org/10.1016/j.quageo.2021.101153.

Klubi, E., Abril, J.M., Nyarko, E., Laissaoui, A., Benmansour, M., 2017. Radioecological assessment and radiometric dating of sediment cores from dynamic sedimentary systems of Pra and Volta estuaries (Ghana) along the Equatorial Atlantic. J. Environ. Radioact. 178–179, 116–126.

Koide, M., Bruland, K.W., Goldberg, E.D., 1973. Th-228/Th-232 and Pb-210 geochronologies in marine and lake sediments. Geochem. Cosmochim. Acta 37 (5), 1171–1187. https://doi.org/10.1016/0016-7037(73)90054-9.

Laissaoui, A., Benmansour, M., Ziad, N., Ibn Majah, M., Abril, J.M., Mulsow, S., 2008. Anthropogenic radionuclides in the water column and a sediment core from the Alboran Sea: application to radiometric dating and reconstruction of historical water column radionuclide concentration. J. Paleolimnol. 40, 823–833.

Lima, A.L., Hubeny, J.B., Reddy, C.M., King, J.W., Hughen, K.A., Eglinton, T.I., 2005. High resolution historical records from Pettaquamscutt River basin sediments: 1. ^{210}Pb and varve chronologies validate record of ^{137}Cs released by the Chernobyl accident. Geochem. Cosmochim. Acta 69, 1803–1812.

Mabit, L., Benmansour, M., Abril, J.M., Walling, D.E., Meusburger, K., Iurian, A.R., Bernard, C., Tarjan, S., Owens, P.N., Blake, W.H., Alewell, C., 2014. Fallout ^{210}Pb as a soil and sediment tracer in catchment sediment budget investigations: a review. Earth Sci. Rev. 138, 335–351.

Robbins, J.A., 1978. Geochemical and Geophysical applications of radioactive lead isotopes. In: Nriago, J.P. (Ed.), Biochemistry of Lead in the Environment. Elsevier, Amsterdam, pp. 285–393.

Robbins, J.A., Edgington, D.N., 1975. Determination of recent sedimentation rates in Lake Michigan using ^{210}Pb and ^{137}Cs. Geochem. Cosmochim. Acta 39, 285–304.

Sánchez-Cabeza, J.A., Ruíz-Fernández, A.C., 2012. ^{210}Pb sediment radiochronology: an integrated formulation and classification of dating models. Geochem. Cosmochim. Acta 82, 183–200.

Smith, J.N., 2001. Why should we believe ^{210}Pb sediment geochronologies? J. Environ. Radioact. 55, 121–123.

Tylmann, W., Enters, D., Kinder, M., Moska, P., Ohlendorf, Ch, Porebal, G., Zolitschka, B., 2013. Multiple dating of varved sediments from Lake Łazduny, northern Poland: toward an improved chronology for the last 150 years. Quat. Geochronol. 15, 98–107.